Applied Surface Science 261 (2012) 137–146

Applied Surface Science

journal homepage: www.elsevier.com/locate/apsusc

Exploring the critical dependence of adsorption of various dyes on the degradation rate using Ln^{3+}-TiO_2 surface under UV/solar light

L. Gomathi Devi*, S. Girish Kumar

Department of Post Graduate Studies in Chemistry, Central College City Campus, Dr. Ambedkar Street, Bangalore University, Bangalore 560001, India

ARTICLE INFO

Article history:
Received 7 February 2012
Received in revised form 19 July 2012
Accepted 19 July 2012
Available online 16 August 2012

Keywords:
Lanthanide ion doped TiO_2
Dopant effects
Degradation of anionic dyes
Adsorption and pH effects
Photocatalysis

ABSTRACT

The degradation of structurally different anionic dyes like Alizarin Red S (ARS) Amaranth (AR), Brilliant Yellow (BY), Congo Red (CR), Fast Red (FR), Methyl Orange (MO), and Methyl Red (MR) were carried out using Ln^{3+} (Ln^{3+} = La^{3+}, Ce^{3+} and Gd^{3+}) doped TiO_2 at different pH conditions under UV/solar light. All the anionic dyes underwent rapid degradation at acidic pH, while resisted at alkaline conditions due to the adsorptive tendency of these dyes on the catalyst surface at different pH conditions. Gd^{3+} (0.15 mol%)-TiO_2 exhibited better activity compared to other photocatalyst ascribed to half filled electronic configuration of Gd^{3+} ions. It is proposed that Ln^{3+} serves only as charge carrier traps under UV light, while it also act as visible light sensitizers under solar light. Irrespective of the catalyst and excitation source, the dye degradation followed the order: AR > FR > MO > MR > ARS > BY > CR. The results suggest that pre-adsorption of the pollutant is vital for efficient photocatalysis which is dependent on the nature of the substituent's group attached to the dye molecule.

1. Introduction

Organic compounds are extensively used in industries for multipurpose and represent an increasing environmental danger. The main goal is to achieve complete mineralization of recalcitrant organic compounds to CO_2, H_2O and simple mineral acids or at least to produce less harmful intermediates. The conventional pollutant destructive technologies include biological, thermal and chemical treatments. The former usually requires a long residence time for microorganisms to degrade the pollutant and they can also be affected by substrate toxicity. Thermal treatments present considerable emission of other hazardous compounds and the methods like flocculation, precipitation, adsorption on activated granular carbon, air stripping or reverse osmosis requires a post-treatment to remove the pollutant from the newly contaminated environment [1]. The biological methods although used, have proven to be partially effective for colored effluents, as in the most cases dyes are not adsorbed onto biomass without being really degraded [2]. Ozone and hypochlorite oxidations as well as UV/H_2O_2 processes are efficient decolourization methods, but they are not desirable because of the high cost of equipment, operating costs, and the secondary pollution arising from the residual chlorine [3]. Heterogeneous photocatalysis using TiO_2 semiconductor has been extensively studied in the degradation of organic compounds both in liquid and gaseous phase [4–10]. TiO_2 is mainly used due to its chemical–biological inertness, strong oxidizing power, cost effectiveness and long term stability against photo-chemical corrosion. However, the current bottleneck of TiO_2 is the high degree of charge carrier recombination and its large band gap requires expensive UV light for activation. In this respect, introduction of defects through the doping of Ln^{3+} ions has proven to extend the charge carrier life time by altering the equilibrium concentration of electrons and holes and also induces red shift in the band gap absorption due to the introduction of localized electronic energy levels by the dopants within the band gap states of TiO_2 [11–25]. In any photocatalytic degradation process, pH of the solution, nature of the substrate, charge on the catalyst surface, dye concentration, concentration of defects and surface-electronic properties of the catalyst will exert their individual effect on the degradation rate. The importance of choosing these parameters is critical for the practical application in photocatalytic oxidation processes. Hence, the present research work focuses on the fundamental issues of photocatalytic degradation process in an aqueous solution using TiO_2 and Ln^{3+} (Ln^{3+} = La^{3+}, Ce^{3+} and Gd^{3+})-TiO_2 under UV/solar light. A series of structurally different anionic dyes like ARS, AR, BY, CR, FR, MO, and MR were chosen in order to investigate the structural correlation of the pollutants on the degradation kinetics (Fig. 1).

2. Experimental

2.1. Preparation of photocatalyst

Polycrystalline anatase TiO_2 was synthesized by sol–gel route through the hydrolysis of titanium tetrachloride [26]. In a typical

* Corresponding author. Tel.: +91 80 22961336.
E-mail address: gomatidevi_naik@yahoo.co.in (L.G. Devi).

0169-4332/$ – see front matter © 2012 Elsevier B.V. All rights reserved.
http://dx.doi.org/10.1016/j.apsusc.2012.07.121

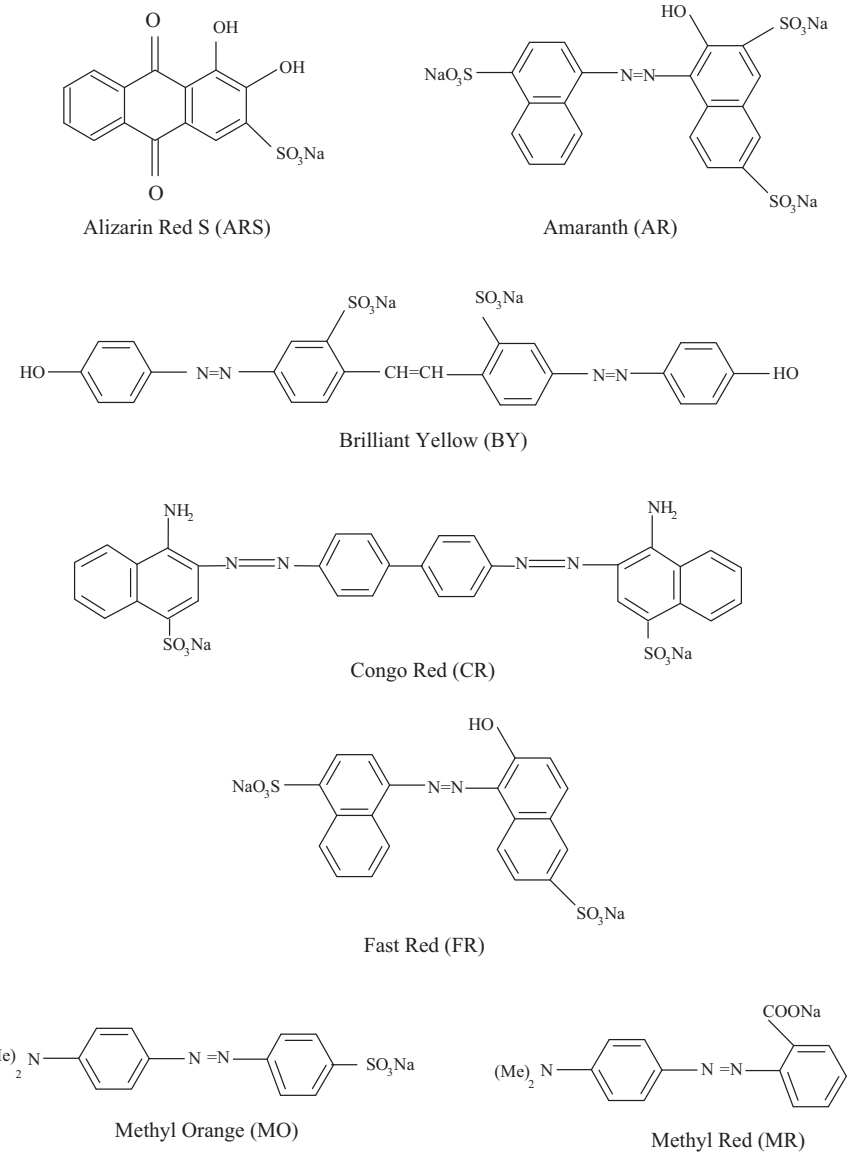

Fig. 1. Schematic representation of different anionic dyes.

procedure, 25 mL of diluted $TiCl_4$ (100 mL of concentrated $TiCl_4$ was diluted to 1 L) with 1 mL concentrated H_2SO_4 is taken in a beaker and diluted to1 L. The pH of the solution was increased to 7–8 by the addition of liquor ammonia. The titanium hydroxide gel precipitate obtained is washed with double distilled water to free from chloride and ammonium ions. The gel was filtered, dried in an oven to remove adsorbed water molecules and then ground to a fine powder to give a xerogel sample, which on calcination at 600° C for 6 h results in pure anatase phase [26]. For the preparation of lanthanide ion doped TiO_2 (Ln^{3+}-TiO_2, Ln = La, Ce and Gd), a known concentration of the metal ion solution was added to calculated amount of anatase TiO_2 to get the dopant concentration in the range of 0.05 to 0.2 mol% (For instance, 1 g of TiO_2 requires 0.00271 g of $Gd_2(CO_3)_2$ to obtain 0.05 mol% of Gd^{3+}). The obtained powder is ground in a mortar, dried and finally calcined at 600° C for 6 h [27].

2.2. Analytical instruments used for characterization of the photocatalysts

The crystalline structure and variation in the lattice parameters of titania and modified titania were determined by powder X-ray diffraction (PXRD) measurements using Philips powder diffractometer PW/1050/70/76 with Cu Kα radiation. The average crystallite size of the sample was calculated using Scherer's equation.

$$D = \frac{k\lambda}{\beta \cos\theta} \quad (1)$$

where k is the shape factor (~0.9), λ is the X-ray wavelength (0.15418 nm), β is the full width at half maximum (FWHM) of the diffraction line and θ is the diffraction angle. The specific surface area of the powders were measured by dynamic Brunner–Emmet–Teller (BET) method in which N_2 gas was adsorbed at 77 K using Digisorb 2006 surface area, pore volume analyzer Nova Quanta Chrome corporation instrument multipoint BET adsorption system. The diffuse reflectance spectra (DRS) of the photocatalyst sample in the wavelength range of 200–700 nm were obtained by a UV–vis scanning spectrophotometer (31031 PC UV-VIS-NIR instrument) using $BaSO_4$ as reference standard. The band gaps of photocatalysts were calculated by using Kubelka–Munk plot.

2.3. Evaluation of photocatalytic activity for the degradation of various dyes

The photocatalytic activity of all the prepared samples were evaluated in the degradation of dyes under UV/solar light and reaction conditions were optimized to achieve maximum efficiency within the desired interval time. Before the start of the reaction, the catalyst were finely dispersed in 250 mL of the dye solution and stirred in dark for 30 min to ensure adsorption equilibrium of the dye on the catalyst surface under the specified pH conditions. The concentration of the substrate in bulk of the solution at this point was used as the initial value for the further kinetic studies. An artificial medium pressure mercury vapour lamp was used to probe the catalytic activity in the UV region. The photon flux of the light source was 7.75 mW/cm^2 as determined by ferrioxalate actinometry and the emission wavelength was in the range of 350–400 nm with intense peak around 370 nm. The distance between the reactor and the lamp housing was 29 cm. The lamp was warmed for some time to reach constant output before the start of the reaction and all irradiation were carried out under constant stirring in the presence of atmospheric oxygen under laboratory conditions. At given intervals of irradiation, samples were withdrawn from the reaction which were simultaneously centrifuged and filtered through filter paper to separate the catalyst particles. The decrease in the concentration of pollutant was quantified by UV–vis spectrophotometer using Shimadzu UV-1700 PharmaspecUV–vis spectrophotometer. The concentration was calculated for each dye was interpreted by measuring absorbance at its maximum wavelength. The optimized experiments were reiterated under solar light illumination in order to study the influence of excitation wavelength on the degradation process and also to probe the catalytic efficiency in the visible portion of the solar spectrum. The photocatalysis using solar light was performed between 11 a.m. and 2 p.m. during the summer season (May–June) in Bangalore, India. The solar intensity in this period was maximal. The latitude and longitude are 12.58N and 77.38E respectively. The average intensity of sunlight was found to be around 0.753 kW cm^{-2} using solar radiometer.

2.4. Calculation of process efficiency (Φ) and electrical energy per order (E_{Eo}) to evaluate the performance of photocatalytic process

(a) *Process efficiency* (Φ): The 'Φ' is defined as the concentration of the pollutant degraded by the amount of energy in terms of intensity and exposure surface area per time;

$$\Phi = \frac{C_0 - C}{tIS} \quad (2)$$

C_0 is the initial concentration of the dye substrate and C is the concentration at time 't' and ($C_0 - C$) denotes the concentration of the dye degraded in ppm, 'I' is the irradiation intensity 125 W, 'S' denotes the solution irradiated plane surface area 176 cm^2 and 't' represents the irradiation time in minutes. It is measured in terms of ppm per Einstein.

(b) *Electrical energy per order* (E_{Eo}): The degradation of aqueous organic pollutant in a light driven process represents a major fraction of operating costs. Simple figures of merit based on the electric energy consumption (as light energy) can therefore be very useful and informative [28,29]. The appropriate figure of merit is the electrical energy per order (E_{Eo}) and is defined as the number of kWh of electrical energy required to reduce the concentration of pollutant by one order of magnitude 1 m^3 of contaminated water. E_{Eo} can be calculated using following equation:

$$E_{Eo} = \frac{1000Pt}{60V \log(C_i/C_f)} \quad (3)$$

Table 1
Structural characterization of Ln^{3+}-TiO_2 photocatalysts.

Photocatalysts	FWHM × 10^{-3}	D (nm)	d_{101} (Å)	V (Å)^3
TiO_2	4.72	30.06	3.512	135.81
La^{3+} (0.05)-TiO_2	5.22	27.2	3.513	135.97
La^{3+} (0.10)-TiO_2	5.99	23.7	3.514	136.25
La^{3+} (0.15)-TiO_2	7.36	19.3	3.515	136.43
La^{3+} (0.20)-TiO_2	9.17	15.5	3.515	136.56
Ce^{3+} (0.05)-TiO_2	4.91	28.9	3.513	136.94
Ce^{3+} (0.10)-TiO_2	5.51	25.8	3.513	136.06
Ce^{3+} (0.15)-TiO_2	6.10	23.3	3.514	136.20
Ce^{3+} (0.20)-TiO_2	7.21	19.7	3.515	136.91
Gd^{3+} (0.05)-TiO_2	5.00	28.4	3.513	136.37
Gd^{3+} (0.10)-TiO_2	5.17	27.5	3.513	135.99
Gd^{3+} (0.15)-TiO_2	6.15	23.1	3.514	136.09
Gd^{3+} (0.20)-TiO_2	6.30	22.56	3.514	136.14

Note: FWHM = Full Width at Half Maximum; D = Crystallite size; d spacing of (1 0 1) crystal plane; V = Unit cell volume. The concentration of dopant is expressed in mol%. The error bars for d spacing were found to be in the range of ±0.001 to ±0.006.

where P is the power of the light source (kW), t is the irradiation time (min), V is the volume of the reaction solution (200 mL), C_i and C_f are the initial and final pollutant concentration. E_{Eo} is expressed in terms of kWh/kg.

3. Results and discussion

3.1. Characterization of photocatalyst

The reflections in the PXRD patterns of undoped TiO_2 and Ln^{3+}-TiO_2 were indexed only to anatase phase suggesting that the dopant Ln^{3+} ion stabilized pristine anatase crystal structure over a range of dopant concentration (Fig. 2A). This indicates that the polycrystalline growth with different orientations is formed in the anatase crystal and the dopants have successfully incorporated into the host lattice. The diffraction angle of most intense crystal plane (1 0 1) of anatase shifted slightly toward lower angle (Fig. 2B and Table 1). The substitution of Ln^{3+} at the Ti^{4+} lattice sites will have stabilizing effect on the Ti—O bond because more electropositive Ln^{3+} will donate its electron density to O^{2-} ion [30]. Thus the increased electron density will strengthen Ti—O bond and inhibits the phase transformation from anatase to rutile as this polymorphic transition critically requires the cleavage of Ti—O bonds. However in the case of Ln^{3+}-TiO_2, this rupture is rather difficult due to the increased bond strength rendered by Ln^{3+} ions [30]. Furthermore, it is expected that the surrounding Ln^{3+} ions will inhibit the phase transition through the formation of Ti—O—Ln bond. On the other hand, Ln_2O_3 lattice locks the Ti—O species at the interface with TiO_2 domains preventing the rutile nucleation [31]. The crystallite sizes of Ln^{3+}-TiO_2 were smaller compared to undoped titania indicating that the inclusion of Ln^{3+} at Ti^{4+} lattice sites of TiO_2 significantly suppressed the grain growth of anatase phase by providing dissimilar boundaries. This reduction in crystallite size is due to the segregation of the dopant cations at the grain boundary, which inhibits the grain growth by restricting the direct contact of grains [32]. The doping of Ln^{3+} improves the pore stability and also results in poor titania-titania connectivity necessary for the phase transformation to rutile. The crystallite size of anatase titania gradually decreased with increase in the Ln^{3+} concentration (Table 1). It is reported that in the case of metal oxides there is critical value of dispersion capacity, at values lower than which the oxide might become highly dispersed on the support without the formation of a separate crystalline phase. Since, no characteristic peak corresponding Ln_2O_3 and lanthanide titanates were observed in the PXRD patterns, it can be concluded that the rare earth ion doping is below the dispersion capacity.

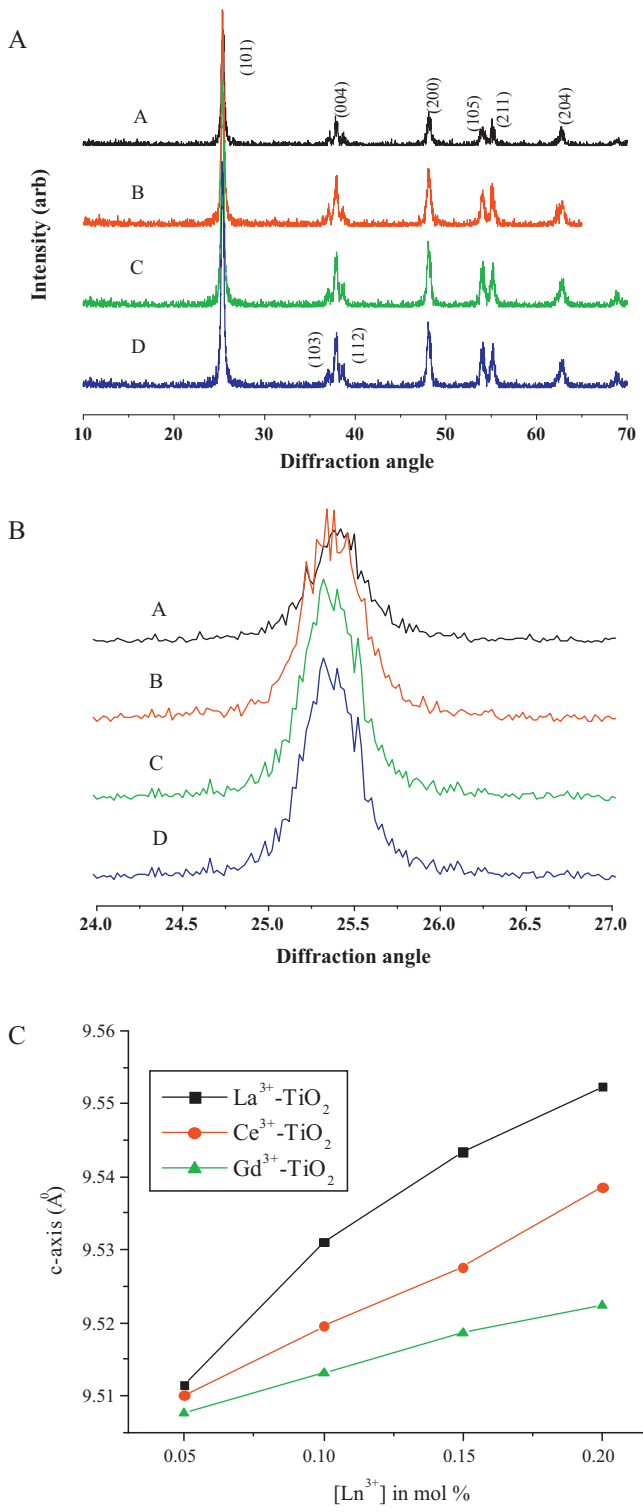

Fig. 2. (A) PXRD patterns of (A) TiO_2; (B) La^{3+} (0.2 mol%)-TiO_2; (C) Ce^{3+} (0.2 mol%)-TiO_2; (D) Gd^{3+} (0.2 mol%)-TiO_2.
(B) PXRD in the slow scanning rate for (A) TiO_2; (B) La^{3+} (0.2 mol%)-TiO_2; (C) Ce^{3+} (0.2 mol%)-TiO_2; (D) Gd^{3+} (0.2 mol%)-TiO_2.
Variation in lattice parameter (*c*-axis) versus dopant concentration in Ln^{3+}-TiO_2.

3.2. Calculation of lattice parameters

The X-ray diffraction peaks of crystal planes (2 0 0) and (2 0 4) in anatase are selected to determine lattice parameters of doped samples using the equations [33];

Bragg's law:

$$d_{hkl} = \frac{\lambda}{2\sin\theta} \quad (4)$$

$$\frac{1}{d_{hkl}^2} = \frac{h^2}{a^2} + \frac{k^2}{b^2} + \frac{l^2}{c^2} \quad (5)$$

d_{hkl} is the distance between crystal planes of ($h\,k\,l$), λ is the X-ray wavelength, θ is the diffraction angle of crystal plane ($h\,k\,l$), $h\,k\,l$ is the crystal plane index and *a*, *b*, *c* are the lattice parameters [33]. For anatase with tetragonal structure, lattice parameters changes to $a = b \neq c$ and hence Eq. (5) modifies to:

$$\frac{1}{d_{hkl}^2} = \frac{h^2 + k^2}{a^2} + \frac{l^2}{c^2} \quad (6)$$

The unit cell volume for the Ln^{3+}-TiO_2 samples were found to be higher than that of undoped TiO_2 due to the higher ionic radius of the dopant Ln^{3+} compared to the host Ti^{4+} ion. The large ionic radii of Ln^{3+} ion induce large degree of local structural polarization with significant lattice expansion for the Ln^{3+}-TiO_2 compared to undoped TiO_2. The lattice expansion increased with increase in the dopant concentration and also with respect to the ionic radius of the dopant (Table 1). The unit cell volume of La^{3+}-TiO_2 (or Ce^{3+}-TiO_2) was higher than Gd^{3+}-TiO_2 due to the higher ionic radius of the La^{3+} (1.15 Å) and Ce^{3+} (1.11 Å) compared to Gd^{3+} (1.02 Å) ion. Since the unit cell volume is almost similar for La^{3+}-TiO_2 and Ce^{3+}-TiO_2, it was assumed that cerium exists in +3 oxidation state. The increase in unit cell volume is attributed to the increase in the ionic radii of Ti ions as electron density move toward the vacant 'd' orbital in the presence of dopants and also to the longer Ln—O bond length compared to the Ti—O bond in pure titania. The variation in the lattice parameters for Ln^{3+}-TiO_2 compared to undoped TiO_2 were reflected in the elongation '*c*' axis, with *a* (=*b*) remaining almost constant in the entire range of dopant concentration. Burns et al. reported that Nd^{3+} dopant in the TiO_2 lattice act as substitutional or interstitial impurity by the changes observed in the variation along the *c*-axis. The authors suggested that Nd^{3+} can act as substitutional impurity up to the dopant concentration of 0.1 mol%, for which maximum elongation in the *c*-axis was observed. For higher dopant concentration (>0.1 mol%), the elongation in *c*-axis remained almost constant suggesting the incorporation of excess Nd^{3+} ions at the interstitial sites [34]. In the present case, elongation in *c*-axis was observed for all the doped samples over the entire range of dopant concentration (Fig. 2C). Since only '*c*' dimension is changing while '*a* (=*b*)' remains almost constant for the range of dopant concentration, it can be concluded that Ln^{3+} substitutes Ti^{4+} preferentially on the bcc and fcc in the anatase structure. The variation in the lattice parameters, decrease of crystallite size and expansion in the unit cell volume for Ln^{3+}-TiO_2 with respect to undoped TiO_2 confirms the possible incorporation of dopant at the lattice Ti^{4+} sites of TiO_2 matrix.

The optical absorption studies indicated red shift in the band gap absorption to the longer wavelength due to the introduction of localized electronic 'f' states of Ln^{3+} ions within the band gap states of TiO_2 that forms the lowest unoccupied molecular orbital [35,36]. Thus the transition for the extrinsic absorption requires lower energy and Ln^{3+}-TiO_2 showed red shift in the band gap absorption compared to undoped TiO_2. The extent of red shift increased with increase in the dopant concentration, with Ce^{3+}-TiO_2 showing large red shift in the band gap absorption compared to La^{3+}-TiO_2 and Gd^{3+}-TiO_2 samples (Fig. 3 and Table 2), as La^{3+} and Gd^{3+} ions possess stable electronic configurations.

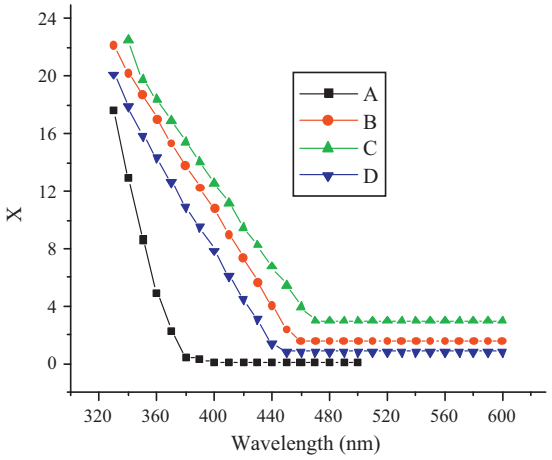

Fig. 3. Kubelka–Munk plot for various photocatalysts (A) TiO_2; (B) La^{3+} (0.2 mol%)-TiO_2; (C) Ce^{3+} (0.2 mol%)-TiO_2; (D) Gd^{3+} (0.2 mol%)-TiO_2. Where $X = (1 - R_\infty)^2/2R_\infty$, R_∞ is ratio of the relative reflectance to reflectance of non absorbing medium, $(1 - R_\infty)^2$ is the molar absorption co-efficient and $2R_\infty$ is the scattering co-efficient.

Table 2
Specific surface area and band gap absorption properties of Ln^{3+}-TiO_2.

Photocatalysts	S (m^2/g)	λ (nm)	E_g (eV)
TiO_2	15	380	–
La^{3+} (0.05)-TiO_2	22	404	0.2
La^{3+} (0.10)-TiO_2	28	428	0.37
La^{3+} (0.15)-TiO_2	37	445	0.41
La^{3+} (0.20)-TiO_2	45	460	0.57
Ce^{3+} (0.05)-TiO_2	19	410	0.24
Ce^{3+} (0.10)-TiO_2	27	435	0.41
Ce^{3+} (0.15)-TiO_2	31	450	0.51
Ce^{3+} (0.20)-TiO_2	37	470	0.63
Gd^{3+} (0.05)-TiO_2	17	395	0.13
Gd^{3+} (0.10)-TiO_2	21	428	0.37
Gd^{3+} (0.15)-TiO_2	25	440	0.45
Gd^{3+} (0.20)-TiO_2	28	450	0.51

Note: S = Specific surface area measured by BET method; λ = band gap absorption of the semiconductors by reflectance spectroscopy; E_g = Position of localized electronic state of the dopant within the band gap states of titania. The concentration of dopant is expressed in mol%.

4. Photocatalytic degradation studies

4.1. Effect of catalyst loading on the dye degradation rate

The effect of catalyst dosage on the photocatalytic degradation of AR dye was studied by varying the amounts of catalyst from 100 to 400 mg/250 mL maintaining the other reaction parameters constant (Fig. 4A and B). Irrespective of the nature of the dyes and photocatalysts, the initial reaction rates were found to enhance linearly with increase in the catalyst dosage up to 250 mg/250 mL indicating the heterogeneous regime. This may probably be due to: (i) increase in the extent of dye adsorption molecules on the catalyst surface; (ii) increase in the number of surface active sites; (iii) enhanced generation of hydroxyl radicals due to increase in the concentration of charge carriers [37]. However, at higher catalyst loadings (400 mg/L), the reaction rate decreased which may be attributed to; (i) the deactivation of activated molecules by collision with ground state molecules; (ii) the agglomeration of the catalyst particles at higher loading which covers the part of photosensitive area retarding the photon absorption and also the dye adsorption; (iii) turbidity at higher catalyst loading results in the shadowing effect thus decreasing the penetration depth of light irradiation; (iv) high degree of scattering by the catalyst particles and increase in the opacity [38,39]. Although, more surface area and more number of surface active sites will be available for the adsorption of dye molecules at higher catalyst loadings, the substrate molecules remain constant in the solution. Hence above a certain level, the additional catalyst amount does not get involved in catalytic activity and further increment in the reaction rate was not observed. The usage of optimum catalyst amount depends on many parameters like geometry of the reactor, nature and concentration of the dye, power of the excitation source and definite amount of TiO_2. The optimization of the catalyst dosage is necessary in order to avoid excess catalyst and also to ensure total absorption of photons for efficient photomineralization.

4.2. Effect of initial dye concentration on the degradation rate

It is important from mechanistic and application point of view to study the dependence of substrate concentration on the photocatalytic degradation rate. The effect of initial AR dye concentration on the degradation rate was investigated in the concentration range 25–100 ppm maintaining the other reaction parameters constant (Fig. 5). Beyond this concentration, degradation rate decreased for all the dyes. This may be due to: (i) higher dye concentration might serve as inner filter shunting the photons away from the catalyst surface; (ii) non availability of oxidative free radicals; (iii) more number of dye molecules get adsorbed on the catalyst surface thus blocking the surface active sites to participate in the degradation reaction [40]. Similar trend was observed for other dyes with catalyst were observed (data not shown).

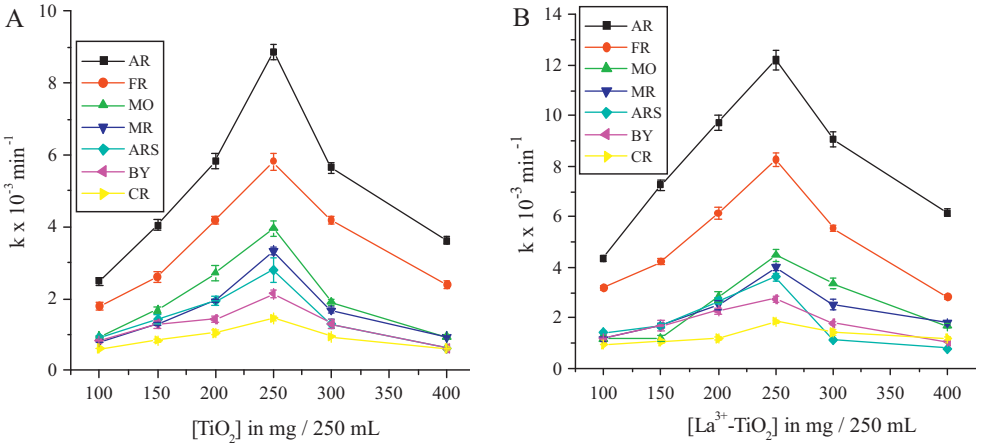

Fig. 4. Rate constant for the degradation of various dyes at different catalyst dosage. (A) TiO_2; (B) La^{3+}-TiO_2.

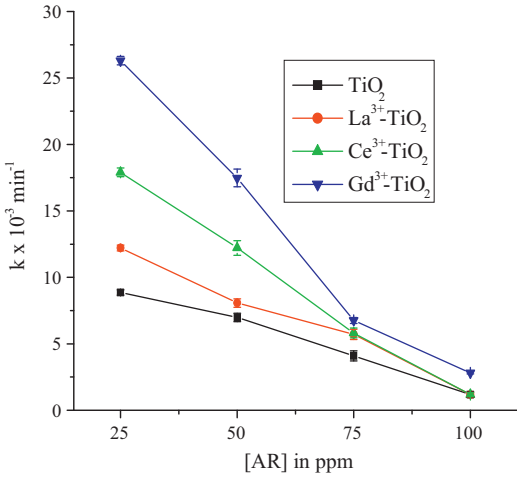

Fig. 5. Rate constant for the degradation at different AR dye concentration using various photocatalysts.

4.3. Existence of optimum dopant concentration within the TiO_2 matrix to show high activity

Ln^{3+}-TiO_2 showed superior activity for the degradation of all the dyes compared to undoped TiO_2 indicating that the dopant induced defects were in the favor of photocatalytic reactions. The positive role of dopant in Ln^{3+}-TiO_2 is attributed to: (i) introduction of mid band gap states by the dopants serving as effective charge carrier traps; (ii) altering the surface acid–base properties of the catalyst thus enhancing the extent of adsorption of the pollutant molecules on the catalyst surface. Irrespective of the nature of the dopant, the photocatalytic degradation for all the dyes increased with increase in dopant concentration up to 0.15 mol% and a drastic decrease was observed at higher dopant concentration (Fig. 6). This result suggests that there exist an optimum dopant concentration within the titania matrix for the efficient separation of charge carriers. Pleskov reported that the value of space charge region potential for the effective separation of photogenerated charge carriers must not be lower than 0.2 eV [41]. On the other hand, the thickness of space charge layer is influenced by the dopant concentration according to the following equation [41,42]:

$$W = \left(\frac{2\varepsilon\varepsilon_0 V_s}{eN_d}\right)^{1/2} \quad (7)$$

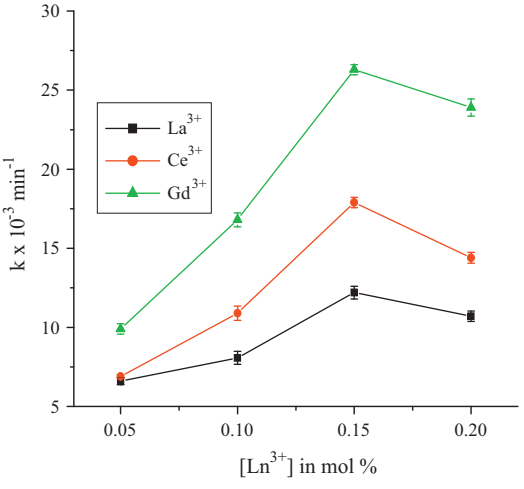

Fig. 6. Rate constant for the degradation of AR using Ln^{3+}-TiO_2 at different dopant concentration.

Where '*W*' is the thickness of space charge layer, ε and ε_0 are the static dielectric constants of the semiconductor and of the vacuum, V_s is the surface potential, N_d is the number of dopant atoms, and e is the electronic charge. Thus it is clearly shown that '*W*' is inversely proportional to dopant concentration in the titania matrix. In addition, penetration depth '*l*', of the light into the solid is given by $l = 1/a$, where '*a*' is the light absorption coefficient at a given wavelength. When the value of '*W*' approximates that of '*l*', all the photon absorbed generate electron–hole pair that are efficiently separated [42]. Consequently, it is understandable that the existence of optimum value of N_d for which a space charge region exist whose potential is not less than 0.2 eV and the thickness is more or less equal to the light penetration depth. The space charge region becomes very narrow for higher dopant concentration (0.2 mol%) and the penetration depth of light into TiO_2 lattice greatly exceeds the thickness of the space charge layer facilitating charge carrier recombination [43]. The small crystallite size of Ln^{3+}-TiO_2 at higher dopant concentration results in the generation of charge carriers sufficiently close to the surface which undergoes rapid surface recombination due to the abundant trapping sites and the lack of driving force to separate these charge carriers. Since Ln^{3+} can serve as trapping sites for both electrons and holes, the possibility of trapping both the charge carriers will be high at higher dopant concentration and this trapped charge carriers may recombine through quantum tunneling [44]. Moreover, the trapped charge carriers may be deeply trapped more than once on its way to surface, reducing the mobility which recombines with its counterpart so that the overall dopant effects will be detrimental on photocatalytic efficiency [44]. The interaction of CB electron with dense internal surface states of the dopants may strongly influence the electron diffusion process, so that the diffusion of charge carriers is drastically reduced resulting in recombination. The charge carriers trapped in such internal surface states are commonly referred to as deep trap states, wherein the subsequent release of charge carriers becomes extremely difficult. The mobility of photoelectrons trapped in these deep surface states is much slower than that of electrons relaxed in shallow traps. At this stage, only a part of photoelectrons, including those released from shallow surface states migrates to the surface initiating dioxygen reduction [45]. Another pathway for recombination arises from the trapped minority carrier in deep surface states recombining with majority carrier resulting in a null reaction. Therefore for any photocatalyst to be photoactive, it should be associated with fewer surface and inner defects. Thus, it is understandable that the appearance of an optimal dopant concentration in the TiO_2 lattice is the balance of increased shallow trapping sites, leading to efficient trapping and fewer deep trapped carriers leading to longer lifetimes for interfacial charge transfer process. Therefore, there is a need for optimal dopant concentration in the TiO_2 matrix to get effective crystallite size for highest photocatalytic efficiency. Beyond the optimum dopant concentration, the rate of recombination dominates the reaction in accordance with the Eq. (8);

$$K_{RR}\alpha \exp\left(\frac{-2R}{a_0}\right) \quad (8)$$

where K_{RR} is the rate of recombination, R is the distance separating the electron and hole pair, a_0 is the hydrogenic radius of the wave function for the charge carrier [46]. As a consequence, the recombination rate increases exponentially with the dopant concentration, since the average distance between the trap sites decreases with increase in the dopant density confined within a particle.

Among the Ln^{3+}-TiO_2 samples, Gd^{3+}-TiO_2 at optimum dopant concentration showed superior activity compared to Ce^{3+}-TiO_2 and La^{3+}-TiO_2 suggesting that the Ln 4f electronic configuration plays an important role in interfacial charge transfer process. Choi et al. systematically studied the effect of doping different metal ions into

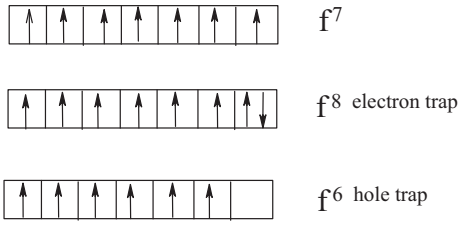

Fig. 7. Schematic representation of Gd^{3+} ion inside the titania matrix serving as trapping electron and hole traps.

quantum sized-TiO_2 matrix for $CHCl_3$ oxidation and CCl_4 reduction [46]. The higher activity for Fe^{3+}-TiO_2 compared to other metal ion doped samples was attributed to unique stable half filled electronic structure of Fe^{3+} ion which was predicted to serve as shallow traps for the charge carriers. Xu et al. also reported the enhanced activity of Gd^{3+}-TiO_2 for the decomposition of nitrate compared to other rare earth doped samples due to the stable half filled electronic configuration of Gd^{3+} ion [47]. This argument supports the higher activity of Gd^{3+}-TiO_2 compared to other photocatalysts for the degradation of all the dyes (Table S1 – supplementary material).

The dopant inside the TiO_2 matrix can serve as electron trap if its energy level is just below the CB or hole trap if its energy level is just above the VB. Gd^{3+} has unique half filled valence electronic configuration of $4f^7$. When Gd^{3+} ions traps electron/hole, there will be considerable loss of spin energy due to change in spin state from high spin (seven unpaired electrons) to low spin (six unpaired electrons) as shown in Fig. 7. According to crystal field theory, both the spin states are highly unstable, the trapped charge carriers by the Gd^{3+} ion in the titania matrix will be detrapped to the surface adsorbed species to restore its stable half filled electronic configuration [48]. If Gd^{3+} traps electron, it get reduced to Gd^{2+}. The trapped electron will be transferred to oxygen molecule promoting the superoxide radical formation;

$$Gd^{3+} + e^- \rightarrow Gd^{2+} \quad (9)$$

$$Gd^{2+} + O_{2\,ads} \rightarrow Gd^{3+} + O_2{}^{\bullet -} \quad (10)$$

$$O_2{}^{\bullet -} + 2H^+ \rightarrow 2OH^{\bullet} \quad (11)$$

If Gd^{3+} is assumed to behave as hole trap, it get oxidized to Gd^{4+}. The trapped holes may be transferred to hydroxyl anion adsorbed on the catalyst surface leading to the formation of hydroxyl radical or it can also be transferred to adsorbed dye molecule to form dye radical.

$$Gd^{3+} + h^+ \rightarrow Gd^{4+} \quad (12)$$

$$Gd^{4+} + OH^- \rightarrow Gd^{3+} + OH^{\bullet} \quad (13)$$

$$Gd^{4+} + dye_{ads} \rightarrow Gd^{3+} + dye^+ \quad (14)$$

These processes not only accelerate interfacial charge transfer kinetics, but also enhance the generation of potential oxidative species like superoxide and hydroxyl radicals. Ln^{3+} being strong Lewis acid, is apparently superior to oxygen molecule in trapping CB electrons [49]. On the other hand, the substitution of Ln^{3+} at the lattice sites of Ti^{4+} results in the formation of Ti^{3+} for charge compensation ($3Ti^{4+} \rightarrow 3Ln^{3+} + Ti^{3+}$) which can also form defect level and act as hole-traps promoting the charge transfer.

$$Ti^{4+}\text{—}O\text{—}H^- + e^- \rightarrow Ti^{3+}\text{—}O\text{—}H^- \quad (15)$$

$$Ti^{3+}\text{—}O\text{—}H^- + h^+ \rightarrow Ti^{4+}\text{—}O\text{—}H^{\bullet} \quad (16)$$

The formation of Ti^{3+} states may cause more oxygen defects which facilitate the efficient adsorption of oxygen on titania surface. The formation of $O_2{}^-$ resulting from the chemisorption of oxygen requires the presence of surface defect site whose concentration can be enhanced by Ln^{3+} doping. The concentration of Ti^{3+} centers increases with increase in the dopant density within the titania matrix and hence these defect level would serve as the recombination centers at very high Ti^{3+} content. Furthermore, trapped electron (Gd^{2+}) and trapped hole (Gd^{4+}) at Gd^{3+} site can also recombine with free hole and free electron respectively to decrease the activity of Gd^{3+}-TiO_2 at higher dopant concentration.

$$Gd^{2+} + h^+ \rightarrow Gd^{3+} \quad (17)$$

$$Gd^{4+} + e^- \rightarrow Gd^{3+} \quad (18)$$

4.4. Influence of pH on the adsorption and degradation of the dyes

The interpretation of pH effect can be principally explained by the modification of electrical double layer at the solid–electrolyte interface, which consequently affects the adsorption–desoprtion processes and the separation efficiency of charge carriers at the surface of semiconductor particles. pH is a complex parameter as it is related to several factors like: (i) charge on the catalyst surface; (ii) size of the particle aggregate formed; (iii) nature of the dye – cationic/anionic/neutral; (iv) magnitude of the substrate adsorption on catalyst surface, (v) band edge position of the semiconductor. The point of zero charge (pzc) of TiO_2 is widely reported to be 6.25. Thus, the surface charge density of TiO_2 will be positive below the pzc and negative above it [50]. In general, the adsorption of the pollutant molecule on the catalyst surface is the result of subtle balance of different effects including the polar/hydrophilic character of the molecule/substrate, solid surface charge and state. The hydroxylated titania can be protonated under acidic conditions and deprotanated under alkaline conditions:

$$TiOH + H^+ \leftrightarrow TiOH_2{}^+ \quad (19)$$

$$TiOH + OH^- \leftrightarrow TiO^- + H_2O \quad (20)$$

Hence it can be concluded that the positively charged TiO_2 surface favors the adsorption of negatively charged molecules and vice versa. The interpretation of pH effects on the degradation process is rather complex as it includes several factors such as (i) electrostatic interaction between the catalyst surface and the dye molecules; (ii) reaction of superoxide and hydroxyl radicals formed on the catalyst surface with the dyes; (iii) concentration of hydroxyl radical generation.

Dye solution (250 mL of 25 ppm) along with 250 mg of the photocatalyst was stirred in dark for 30 min and the amount of dye adsorption on the catalyst surface was calculated by comparing the concentration before and after stirring. The percentage adsorption was calculated using the formula;

$$\frac{(C_0 - C)}{C_0} \times 100 \quad (21)$$

where C_0 and C represent the concentration of the dye molecules before and after stirring. The adsorption trend of the dyes on the catalyst surface at different pH conditions showed the following order irrespective of the nature of the catalysts;

At pH 2.5 and 5.0: AR > FR > MO > MR > ARS > BY > CR.

Ln^{3+}-TiO_2 showed better adsorption capacity for all the dyes compared to undoped TiO_2. For a given dye, the adsorptive capacity of the Ln^{3+}-TiO_2 with respect to the dopant concentration followed the order: 0.2 > 0.15 > 0.1 > 0.05 > 0.00 mol% which is analogous trend with the surface area of the catalyst. It is well known that Ln^{3+} ions are known for their ability to form complexes with various Lewis bases (e.g. amines, aldehydes, thiols, alcohols, etc.) via the interaction of these functional groups with vacant f-orbital of Ln^{3+} ion. Thus incorporation of Ln^{3+} at the Ti^{4+} lattice sites of

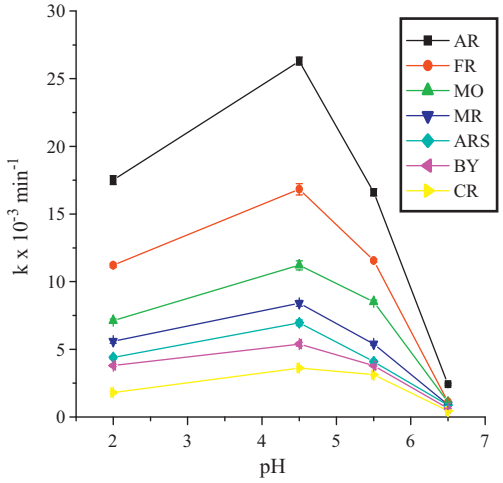

Fig. 8. Rate constant for the degradation at different dye under different pH conditions using Gd^{3+}-TiO_2.

TiO_2 matrix provides a means to concentrate the organic pollutants at the semiconductor surface [15–20]. The substitution of Ln^{3+} results in a modification of energy distribution and strength of surface adsorption sites. The increment of surface acidity in Ln^{3+}-TiO_2 is generally associated with heterometallic bonding Ti—O—Ln formation. In this case, the formation of Ti—O—Ln bond is accompanied by the generation of lattice and surface defects which can act as strong acid sites. Sibu et al. suggested that surface adsorption reactive acidic sites increases with increases in La^{3+} content in the TiO_2 matrix [30]. Hence the surface acidity and the larger surface area of Ln^{3+}-TiO_2 compared to pure TiO_2 results in higher amount of dye adsorption. It is also reported that the Ln^{3+}-TiO_2 provides more adsorption sites and also induce surface states which enables the dye molecule to adsorb more efficiently [30]. The rate constant calculated for the degradation of dyes using La^{3+}-TiO_2 catalysts at different pH conditions are shown in Fig. 8. Evidently, adsorption of various dyes through their functional groups on the catalyst surface found to have a positive correlation on the degradation rate. The properties of the pollutants like functional groups (reactive groups), substituent attached, localized electronic density, possibility of binding to surface atoms to make covalent bonds plays a vital role in driving the adsorption phenomenon. Because the recombination of photogenerated electron and hole is so rapid, interfacial electron transfer is a kinetically competitive process only when the donor or acceptor is preadsorbed on the catalyst surface. The degradation of mono azo dyes was faster compared to di azo dyes under acidic pH. Among the mono azo dyes, AR showed higher rate constant for degradation compared to MO, MR, and FR which is directly related to the nature of the substituent group attached on the dye molecule. Under acidic pH, the catalyst surface will be positively charged and contains more surface acidic sites. The Lewis base property of anionic dyes renders the molecule to get adsorbed more easily on the catalyst surface. The presence of more number of negatively charged acidic sulfonate group on AR drives the molecule to adsorb strongly on catalyst surface and hence undergoes faster degradation. Due to the favorable dimension and spatial geometry, sulfonate group co-ordinates to the surface Ti(IV) centers through sulphonilic oxygen accompanied by the substitution of surface coordinated —OH moieties of ≡Ti—OH [51,52]. Because of the strong overlap between 3d orbitals of the Ti (IV) atoms and 2p orbitals of oxygen, the formation of Ti—O bonds would have strong covalent character (Fig. 9A and B). The rate constant calculated for the degradation of AR is higher than FR despite the fact that both sulfonate and hydroxyl groups were also present on FR. AR can anchor on the titania surface via two ways: (i) the two sulfonate ring attached on the naphthalene moiety can make a covalent bond with surface Ti^{4+} and dopant Ln^{3+} ions (or with two surface Ti^{4+} ions as shown arbitrarily in the Fig. 9); (ii) sulfonate and hydroxyl groups attached on the neighboring carbon can also anchor either on Ln^{3+} or Ti^{4+} ions rendering the stronger adsorption and complex formation of both the functional groups due to the favorable stereo configuration of AR compared to other dyes. While in the case of FR, orientation of dye molecule can be such that only one group either sulfonate or hydroxy can be adsorbed on the catalyst surface. Due to the strong tendency of sulfonate to co-ordinate with Ti(IV) compared to —OH group, it is reasonable to speculate that only sulfonate group of FR co-ordinates to the catalyst surface. The rate constant calculated for the degradation of MO is higher compared to MR due to the fact that sulfonate group being more acidic compared to carboxyl group of MR and hence MO shows stronger adsorption and faster degradation rate compared to MR.

Among the diazo dyes, the rate constant calculated for the degradation of BY is higher than the CR dye despite the fact that CR is stronger Lewis base compared to BY. The stearic hindrance arising from the presence of fused aromatic rings of naphthalene and biphenyl moiety resists the adsorption of CR dye on the catalyst surface [53]. In the case of BY, the stearic hindrance from the four bulky aromatic rings is less compared to CR and hence undergoes faster degradation. The di azo dyes showed low rate constant for degradation compared to mono azo dyes probably due to the inertness of two azo bonds for the free radicals attack and low degree of adsorption on the catalyst surface. All the anionic dyes showed lower rate constant at pH 1.5 though stronger adsorption of dyes

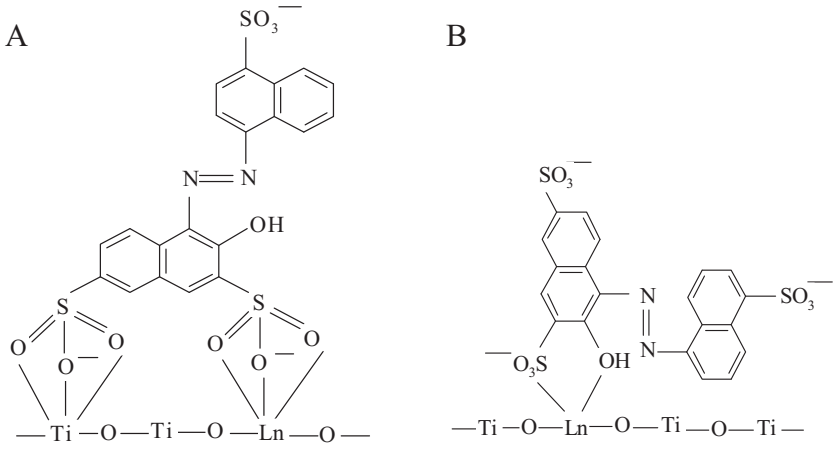

Fig. 9. Probable adsorption modes of AR on the catalyst surface.

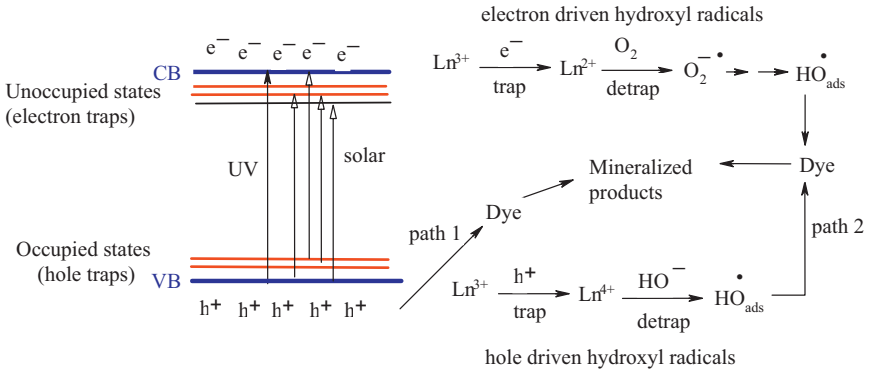

Fig. 10. Mechanistic pathway for the degradation of dye under UV and solar light irradiation. Path 1: direct oxidation of dye molecule by the photogenerated holes. Path 2: degradation of the dye by surface bound hydroxyl radicals.

took place under these conditions. The stronger adsorption of dyes might serve as inner filter shunting the photons away from the catalyst surface thereby preventing the excitation of semiconductor itself and reduce the concentration of charge carriers in the solution. At pH 8.0, the catalyst surface will be negatively charged and hence all the anionic dyes experience electrostatic repulsion resulting in negligible adsorption leading to lowest rate constant (Fig. 8).

4.5. Photocatalytic degradation mechanism of dyes under UV/Solar light using Ln^{3+}-TiO_2

The order of the degradation for various dyes was well correlated with their adsorptive tendency on the catalyst surface. Since the photolysis of the dyes was negligible irrespective of the excitation source, it can be concluded that degradation was due to the combined effects of light source and the catalyst surface. Two distinct mechanisms is proposed under UV/solar light illumination taking into account that the VB edge of the titania will be more positive than the VB edge of dyes and CB edge of dyes will be more negative compared to CB edge of TiO_2 [54]. Under UV light illumination, the electrons are excited from the VB to the CB of TiO_2 leaving behind positively charged hole. The excited electron will be trapped by Ln^{3+}/Ln^{2+} site and subsequent electron transfer to adsorbed O_2 generates superoxide radicals. Ln^{3+} being strong Lewis acid due to the presence of partially filled f-orbital effectively traps CB electron at a faster rate compared to O_2. The VB hole can thus move uphill and oxidize the adsorbed dye leading to complete mineralization (Fig. 10). Photosensitization of the dyes under solar light resulted in ~6–12% degradation of the dyes confirming that the degradation of the dyes through sensitization mechanism was of minor pathway. Under visible light, multiple transitions take place; (i) from occupied states (Ln—O—Ln) to unoccupied states (Ln—O—Ti); (ii) from Ln—O—Ln to CB; (iii) from VB to Ln—O—Ti. Therefore, the quantity of photoinduced charge carriers was much higher than that of pure titania under solar light (Fig. 10). Thus we speculate that the multichannel routes for electron transfer extended the life time for the charge carrier separation under solar light obviously resulting in the higher rate constants compared to UV light (Table S1). However, such electron transfer process also depends on the intensity of the excitation source. It should be noted that the redox reactions occur from both the intrinsic as well as extrinsic photo absorption and it is rather difficult to ascertain the contribution from each of them. These results suggest that the dopant induced electronic states serve only as charge carrier trap under UV light, while it also serves as sensitizer to absorb photons under solar light [55]. The expansion in the crystal matrix creates oxygen vacancies generating shallow energy states at the bottom of the CB which can also serve as reactive electron trapping site. The oxygen vacancies induced by Ln^{3+} in TiO_2 matrix for the charge compensation can be represented by Kroeger–Vink notation:

$$Ln_2O_3 \leftrightarrow 2Ln''_{Ti} + 3Oo + Vo^{\bullet\bullet}/2Vo^{\bullet} \quad (22)$$

Oxygen vacancy refers to the defect states, which are mainly associated with 3d character. This vacancy introduces two localized Ti^{3+} states ~1 eV below the CB edge at concentration of 15% (1 0 1) surface of anatase TiO_2 [56]. When the reaction are carried out in O_2 atmosphere, O_2 adsorbs in these vacancy sites as $O_2^{\bullet-}$, at a ratio of up to three molecules per oxygen vacancy [56]. These vacancies act as effective trapping sites, after the CB electrons relax in these positions. Moreover, the trapped electron reacts more rapidly with O_2 compared to free electrons forming superoxide radicals leading to higher photocatalytic activity. These oxygen vacancies promote the adsorption of O_2 and there exists a strong interaction between the photoinduced electrons bound by oxygen vacancies and adsorbed O_2. This indicated that the binding for photoinduced electrons of oxygen vacancies can capture photoinduced electrons of adsorbed O_2, and O_2 free group was produced at the same time [57,58]. Thus, oxygen vacancies and defects were in favor of photocatalytic reactions and O_2 was active to promote the oxidation of organic dyes.

$$Vo^{\bullet\bullet} + e^- \rightarrow Vo^{\bullet} \quad (23)$$

$$Vo^{\bullet} + O_2 \rightarrow Vo^{\bullet\bullet} + O_2^{\bullet-} \quad (24)$$

Thus the separation of the charge carriers is attributed to such trapping by dopant induced electronic states, defects and high density of oxygen vacancies. Subsequently, the charge carriers migrates to the surface of photocatalyst and participates in the redox reactions enhancing the photocatalytic activity La^{3+}-TiO_2 compared to pure titania.

5. Conclusion

The photocatalytic activity of rare earth ion (La^{3+}, Ce^{3+} and Gd^{3+} ion) doped titania were probed in the degradation of structurally different anionic dyes under UV/solar light. The degradation was found to be strongly dependent adsorption of the dyes on the catalyst surface as well as on the pH of the reaction medium. All the anionic dyes underwent rapid degradation at acidic pH due to electrostatic force of attraction between positively charged catalyst surface and negatively charge dye molecules. Gd^{3+}-TiO_2 showed superior activity for the degradation of all the dyes compared to other photocatalysts, attributed to unique half filled electronic configuration of Gd^{3+} which served as shallow traps for the charge carriers thus enhancing charge separation. The enhanced surface

acidity and induced oxygen vacancies of doped catalysts additionally contributed to overall efficiency. This study highlights that preadsorption of pollutant on the catalyst surface is vital to achieve higher efficiency in titania mediated heterogeneous photocatalysis.

Appendix A. Supplementary data

Supplementary data associated with this article can be found, in the online version, at http://dx.doi.org/10.1016/j.apsusc.2012.07.121.

References

[1] O. Tunay, I. Kabdasli, G. Eremektar, D. Orhon, Water Science and Technology 34 (1996) 9–16.
[2] F.I. Hai, K. Yamamoto, K. Fukoshi, Critical Reviews in Environment Science and Technology 37 (2007) 315–377.
[3] Y. Yoshida, S. Ogata, S. Nakamatsu, T. Shimamune, K. Kikawa, H. Inoue, C. Iwakura, Electrochimica Acta 45 (1999) 409–414.
[4] F. Han, V.S.R. Kambala, M. Srinivasan, D. Rajarathnam, R. Naidu, Applied Catalysis A: General 359 (2009) 25–40.
[5] S.G. Kumar, L.G. Devi, Journal of Physical Chemistry A 115 (2011) 13211–13241.
[6] G. Liu, L. Wang, H.G. Yang, H.M. Cheng, G.Q. Lu, Journal of Materials Chemistry 20 (2010) 831–843.
[7] (a) D. Chattarjee, S. Dasgupta, Journal of Photochemistry and Photobiology C: Photochemistry Review 6 (2005) 186–205;
(b) L.G. Devi, S.G. Kumar, Central European Journal of Chemistry 9 (2011) 959–961;
(c) A.R. Khataee, M.B. Kasiri, Journal of Molecular Catalysis A: Chemical 328 (2010) 8–26.
[8] J. Yu, H. Yu, B. Cheng, C. Trapalis, Journal of Molecular Catalysis A: Chemical 249 (2006) 135–142.
[9] J. Yu, S. Liu, H. Yu, Journal of Catalysis 249 (2007) 59–66.
[10] M.R. Hoffmann, S.T. Martin, W. Choi, D.W. Bahnemann, Chemical Reviews 95 (1995) 69–96.
[11] S. Binham, W.A. Daoud, Journal of Materials Chemistry 21 (2011) 2041–2050.
[12] K.T. Ranjit, I. Wilner, S.H. Bossmann, A.M. Braun, Journal of Catalysis 204 (2001) 305–313.
[13] K.T. Ranjit, I. Wilner, S.H. Bossmann, A.M. Braun, Environmental Science and Technology 35 (2001) 1544–1549.
[14] F.B. Li, X.Z. Li, M.F. Hou, Applied Catalysis B: Environmental 48 (2004) 185–194.
[15] Y. Zhang, H. Zhang, Y. Xu, Y. Wang, Journal of Materials Chemistry 13 (2003) 2261–2265.
[16] J. Liqiang, S. Xiaojun, X. Baifu, W. Baiqi, C. Weimin, F. Honggang, Journal of Solid State Chemistry 177 (2004) 3375–3382.
[17] X. Quan, Q. Zhao, H. Tan, X. Sang, F. Wang, Y. Dai, Materials Chemistry and Physics 114 (2009) 90–98.
[18] Y.H. Xu, H.R. Chen, Z.X. Zeng, B. Lei, Applied Surface Science 252 (2006) 8565–8570.
[19] M. Luo, J. Chen, L. Chen, J. Lu, Z. Feng, C. Li, Chemistry of Materials 13 (2001) 197–202.
[20] M. Sidheshwaran, L.L. Tavlarides, Industrial and Engineering Chemistry Research 48 (2009) 10292–10306.
[21] D. Falcomer, M. Daldosso, C. Cannas, A. Musinu, B. Lasio, S. Enzo, A. Speghini, M. Bettinelli, Journal of Solid State Chemistry 179 (2006) 2452–2457.
[22] D.C. Romero, G.T. Torres, J.C. Arevalo, R. Gomez, A.A. Elguezbal, Journal of Sol–Gel Science and Technology 56 (2010) 219–226.
[23] J.W. Shi, J.T. Zheng, W. Peng, Journal of Hazardous Materials 161 (2009) 416–422.
[24] L.G. Devi, B.N. Murthy, S.G. Kumar, Journal of Molecular Catalysis A: Chemical 308 (2009) 174–181.
[25] T. Peng, D. Zhao, H. Song, C. Yan, Journal of Molecular Catalysis A: Chemical 238 (2006) 119–126.
[26] L.G. Devi, G.M. Krishnaiah, Journal of Photochemistry and Photobiology A: Chemistry 121 (1999) 141–145.
[27] L.G. Devi, B.N. Murthy, S.G. Kumar, Catalysis Letters 130 (2009) 496–503.
[28] N. Daneshvar, A. Aleboyeh, A.R. Khataee, Chemosphere 59 (2005) 761–767.
[29] J.R. Bolton, K.G. Bircger, W. Tumas, C.A. Tolman, Pure and Applied Chemistry 73 (2001) 627–637.
[30] C.P. Sibu, S.R. Kumar, P. Mukundan, K.G.K. Warrier, Chemistry of Materials 14 (2002) 2876–2881.
[31] J. Lin, J.C. Yu, Journal of Photochemistry and Photobiology A: Chemistry 116 (1998) 63–67.
[32] Y. Zhang, H. Xu, Y. Xu, H. Zhang, Y. Wang, Journal of Photochemistry and Photobiology A: Chemistry 170 (2005) 279–285.
[33] J.C. Yu, J. Lin, R.W.M. Kwok, Journal of Physical Chemistry B 102 (1998) 5094–5098.
[34] A. Burns, G. Hayes, W. Li, J. Hirvonen, J.D. Demaree, S.I. Shah, Materials Science and Engineering B 111 (2004) 150–155.
[35] W. Li, Y. Wang, S.I. Shah, C.P. Huang, D.J. Doren, S.A. Rykov, J.G. Chen, M.A. Barteau, Applied Physics Letters 83 (2003) 4143–4145.
[36] Q. Xiao, Z. Si, J. Zhang, C. Xiao, X. Tan, Journal of Hazardous Materials 150 (2008) 62–67.
[37] A.P. Toor, A. Verma, C.K. Jotshi, P.K. Bajpai, V. Singh, Dyes and Pigments 68 (2006) 53–60.
[38] K. Nagaveni, G. Sivalingam, M.S. Hegde, G. Madras, Applied Catalysis B: Environmental 48 (2004) 83–93.
[39] M. Saquib, M. Muneer, Dyes and Pigments 53 (2002) 237–249.
[40] M. Saquib, M. Muneer, Dyes and Pigments 56 (2003) 37–49.
[41] Y. Pleskov, Soviet Electrochemistry 17 (1981) 1–25.
[42] L. Palmisano, V. Augugliaro, A. Sclafani, M. Schiavello, Journal of Physical Chemistry 92 (1988) 6710–6713.
[43] K.E. Karakitsou, X.E. Verykios, Journal of Physical Chemistry 97 (1993) 1184–1189.
[44] Z. Zhang, C.C. Wang, R. Zakaria, J.Y. Ying, Journal of Physical Chemistry B 102 (1998) 10871–10878.
[45] J. Yu, G. Dai, B. Huang, Journal of Physical Chemistry C 113 (2009) 16394–16401.
[46] W. Choi, A. Termin, M.R. Hoffmann, Journal of Physical Chemistry 98 (1994) 13669–13679.
[47] A.W. Xu, Y. Gao, H.Q. Liu, Journal of Catalysis 207 (2002) 151–157.
[48] (a) L.G. Devi, S.G. Kumar, B.N. Murthy, N. Kottam, Catalysis Communications 10 (2009) 794–798;
(b) L.G. Devi, N. Kottam, S.G. Kumar, Journal of Physical Chemistry C 113 (2009) 15593–15601;
(c) L.G. Devi, N. Kottam, B.N. Murthy, S.G. Kumar, Journal of Molecular Catalysis A: Chemical 328 (2010) 44–52;
(d) L.G. Devi, S.G. Kumar, Applied Surface Science 257 (2011) 2779–2790;
(e) L.G. Devi, B.N. Murthy, S.G. Kumar, Materials Science and Engineering B 166 (2010) 1–6;
(f) L.G. Devi, N. Kottam, S.G. Kumar, K.S.A. Raju, Catalysis Letters 131 (2009) 612–617;
(g) J. Yu, Q. Xiang, M. Zhou, Applied Catalysis B: Environmental 90 (2009) 595–602;
(h) M. Zhou, J. Yu, B. Cheng, Journal of Hazardous Materials 137 (2006) 1838–1847.
[49] T. Tong, J. Zhang, B. Tian, F. Chen, D. He, M. Anpo, Journal of Colloid and Interface Science 315 (2007) 382–388.
[50] A. Houas, H. Lachheb, M. Ksibi, E. Elaloui, C. Guillard, J.M. Herrmann, Applied Catalysis B: Environmental 31 (2001) 145–157.
[51] R. Comparelli, E. Fanizza, M.L. Curri, P.D. Cozzoli, G. Mascoio, R. Passino, A. Agostiano, Applied Catalysis B: Environmental 55 (2005) 81–91.
[52] C. Bauer, P. Jacques, A. Kalt, Chemical Physics Letters 307 (1999) 397–406.
[53] L.G. Devi, B.N. Murthy, S.G. Kumar, Chemosphere 76 (2009) 1163–1166.
[54] T. Wu, G. Liu, J. Zhao, H. Hidaka, N. Serpone, Journal of Physical Chemistry B 102 (1998) 5845–5851.
[55] N. Murakami, T. Chiyoya, T. Tsubota, T. Ohno, Applied Catalysis A: General 348 (2008) 148–152.
[56] A. Fujishima, X. Zhong, D.A. Tryk, Surface Science Reports 63 (2008) 515–582.
[57] J. Liqiang, X. Xiaojun, X. Baifu, W. Baiqi, C. Weimin, F. Honggang, Journal of Solid State Chemistry 177 (2004) 3375–3382.
[58] Q. Xiao, Z. Si, Z. Yu, G. Qiu, Materials Science and Engineering B 137 (2007) 189–194.